

# Stability of Statics Aware Voronoi Grid-Shells

D. Tonelli<sup>a,\*</sup>, N. Pietroni<sup>b</sup>, E. Puppo<sup>c</sup>, M. Froli<sup>a</sup>, P. Cignoni<sup>b</sup>,  
G. Amendola<sup>d</sup>, R. Scopigno<sup>b</sup>

<sup>a</sup>*University of Pisa, Department DESTeC, Pisa - Italy*

<sup>b</sup>*VCLab, CNR-ISTI, Pisa - Italy*

<sup>c</sup>*University of Genova, Department Dibris, Genova - Italy*

<sup>d</sup>*University eCampus, Via Isimbardi 10 - 22060 Novedrate (CO) - Italy*

---

## Abstract

Grid-shells are lightweight structures used to cover long spans with few load-bearing material, as they excel for lightness, elegance and transparency. In this paper we analyse the stability of hex-dominant free-form grid-shells, generated with the *Statics Aware Voronoi Remeshing* scheme introduced in Pietroni et al. (2015). This is a novel hex-dominant, organic-like and non uniform remeshing pattern that manages to take into account the statics of the underlying surface. We show how this pattern is particularly suitable for free-form grid-shells, providing good performance in terms of both aesthetics and structural behaviour. To reach this goal, we select a set of four contemporary architectural surfaces and we establish a systematic comparative analysis between Statics Aware Voronoi Grid-Shells and equivalent state of the art triangular and quadrilateral grid-shells. For each dataset and for each grid-shell topology, imperfection sensitivity analyses are carried out and the worst response diagrams compared. It turns out that, in spite of the intrinsic weakness of the hexagonal topology, free-form Statics Aware Voronoi Grid-Shells are much more effective than their state-of-the-art quadrilateral counterparts.

### *Keywords:*

Grid-shells, topology, Voronoi, free-form, imperfection sensitivity, buckling, equivalent continuum

---

\*Corresponding author

*Email address:* [davide.tonelli@dic.unipi.it](mailto:davide.tonelli@dic.unipi.it) (D. Tonelli)

## 1. Grid-shells: topology and stability

Grid-shells, also called lattice shells or reticulated shells, belong to the category of *lightweight structures*. The shape of these structures is optimized to support its own weight, its geometry being modified to provide additional stiffness to the overall structure.

Unfortunately, they are as efficient as exposed to risky buckling phenomena. In fact, in terms of structural behaviour grid-shells are akin to shells but, at the same time, they are lighter and more flexible, hence even harder to analyse.

Shells typically suffer from modes interaction (i.e. some of the first linear buckling factors are coincident or have little separation) and imperfection sensitivity (i.e. a slight perturbation of their curvature may produce an unexpected deterioration of their static behaviour). Both these phenomena are extremely detrimental and usually lead to a huge abatement of the theoretical linear buckling load of the perfect shell Koiter (1967); Hutchinson (1967).

The same phenomena are usually less pronounced for grid-shells, although still present and indeed dangerous Gioncu (1995). This is because the collapse load is more likely to be determined by limit point rather than by bifurcation of equilibrium.

In particular the grid-shell topology (together with the surface curvature) determines the ratio between extensional and inextensional internal strain energy, and thus the failure mode. For example section 6.1 shows how usually

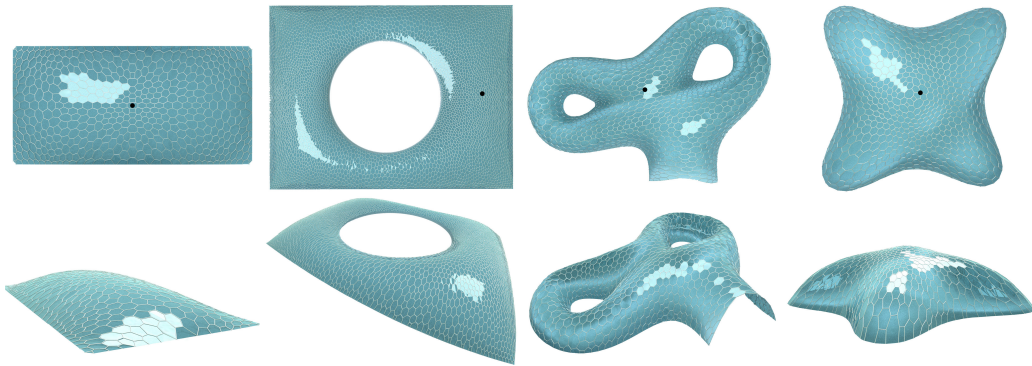


Figure 1: All Datasets. From left to right respectively: *Neumünster Abbey* glass roof, *British Museum* great court glass roof, *Aquadom* and *Lilium Tower* architectural free form shapes. The black bullet is the state parameter adopted in the geometrically non-linear analyses.

23 an unstable symmetric bifurcation point appears in conjunction with trian-  
24 gular topology and quasi-funicular underlying surface with regular boundary,  
25 whereas limit points are usually associated with higher order topologies.

26 Analytical relationships are available for the calculation of the linear buck-  
27 ling load for shells of some shapes and restraint conditions Timoshenko and  
28 Gere (1961), together with experimental knockdown factors for abating the  
29 linear unsafe values Weingarten et al. (1968), as a result of the efforts of the-  
30 oretical and industrial research carried out since the end of the XIX century.  
31 Unfortunately, no akin results are available for grid-shells.

32 Some attempts were done to evaluate the equivalent membrane stiffness and  
33 thickness of planar grids, in order to estimate the buckling load of grid-shells  
34 by using the available relationships for continuous shells Wright (1965); For-  
35 man and Hutchinson (1970). Although overestimating the real buckling load  
36 and totally disregarding imperfections and material non-linearity Sumec and  
37 Zingali (1987); Gioncu (1995), the equivalent continuum method is very use-  
38 ful at least in the preliminary phase of the assessment process. Unfortunately,  
39 analytical solutions are available for a finite set of continuum shells, thus lim-  
40 iting its application. As a consequence, fully non-linear numerical analyses  
41 are the standard tool for the assessment of the stability of grid-shells.

42 From a geometrical point of view, grid-shells can be considered as the  
43 discretization of continuous shells: the continuous shape is tessellated by  
44 a set of connected piecewise linear modules composing a manifold mesh.  
45 It is evident that both curvature and meshing influence the statics of the  
46 structure, but while the effect of curvature can be somehow envisaged with  
47 the theory of shells Timoshenko and Gere (1961), the outcome of meshing  
48 is much more difficult to predict and additionally few related studies are  
49 available (Adriaenssens et al., 2014, p. 239-244).

50 In summary, the behaviour of a grid-shell is utterly affected by the *Gaus-*  
51 *sian curvature* of its underlying surface, the *grid topology*, the *grid spac-*  
52 *ing*, the *beam cross section*, the *joint stiffness* and the (potential) *stiffening*  
53 *method* Malek and Williams (2013); Gioncu (1995).

54  
55 Up to now, many examples of glass covered grid-shells have been built,  
56 the vast majority of which being designed with triangular and quadrilateral  
57 grid topologies Schlaich and Schober (1994, 1996, 1997). Triangular grid-  
58 shells are unanimously credited as the most statically efficient structures as  
59 they rely on extensional deformation only, whereas quadrilateral grid-shells  
60 provide a better trade-off between statics efficiency, transparency and man-

61 ufacturing cost. In fact, quadrilaterals achieve high transparency at equal  
62 weight, as their *area/perimeter* ratio is higher than that provided by trian-  
63 gles. Additionally, planar panels can be easily obtained that, by virtue of  
64 their almost right angles, are easier and cheaper to produce than triangu-  
65 lar panels Glymph et al. (2004); Liu et al. (2006). Unfortunately, quadri-  
66 lateral and polygonal patterns generally undergo inextensional deformation  
67 (i.e. that involves beams bending), that makes them less efficient than their  
68 triangular competitors. As a consequence, most frequently the effective use  
69 of the quadrilateral topology required the adoption of special stiffening meth-  
70 ods (e.g. bracing cables) Schlaich and Schober (2002), whereas higher order  
71 topologies such as the hexagonal are yet highly mistrusted by structural  
72 engineers. This attitude is not totally fair because while hexagonal grids  
73 display an isotropic equivalent mechanical behaviour, quadrilateral grids are  
74 orthotropic and it is demonstrated that their efficiency greatly varies with the  
75 loading direction, becoming even much worse than that of hexagons in the  
76 most unfavourable case Tonelli (2014). This in turn indicates that a grid-shell  
77 with an optimized Voronoi-like topology (i.e. hex-dominant) might display  
78 a very satisfying structural behaviour.

79 In this paper we focus on pinning down the structural behaviour of Statics  
80 Aware Voronoi Grid Shells introduced in Pietroni et al. (2015), that are ac-  
81 tually polygonal hex-dominant grid-shell structures, i.e. composed of mostly  
82 hexagonal faces, including a few generic polygonal faces, usually heptagons,  
83 pentagons and quads. From a purely geometric viewpoint, this kind of struc-  
84 tures turns out to be extraordinarily *adaptive* and suitable for *free form*  
85 *architecture*, definitely much more than purely hexagonal structures Jiang  
86 et al. (2014). In the following, we demonstrate how this pattern can be  
87 successfully used to tessellate *highly free form surfaces* providing static per-  
88 formances that are considerably better than current practice quadrilateral  
89 remeshing schemes, while for quite *regular* geometries the performances are  
90 comparable. This also demonstrates how the ‘*statics awareness*’ introduced  
91 in Pietroni et al. (2015) can be adopted to overcome the intrinsic structural  
92 weakness of polygonal topologies.

93 For the sake of brevity in the proposed experiments we considered no  
94 stiffening method (e.g. bracing cables). As a consequence all the beams’  
95 joints have been modeled as rigid (see section 5.1 for more details).

## 96 2. Stability checks for grid-shells

97 Grid-shells are compressive structures and consequently they can display  
98 several types of stability failure Gioncu (1995); Bulenda and Knippers (2001):

- 99 1. **member buckling:** the classic Euler beam buckling under concentric  
100 axial load;
- 101 2. **node instability:** a set of beams fails locally due to the snap through  
102 of a node;
- 103 3. **line instability:** all nodes of a ring in a dome or a generatrix of a barrel  
104 vault buckle simultaneously (less determinant for free-form shapes);
- 105 4. **global instability:** the whole structure undergoes sudden long-wave  
106 displacements.

107 Usually member instability is decisive for high grid spacing values (see section  
108 5.2 for a coherent definition of grid-spacing), whereas global instability and  
109 line instability are more likely to appear in conjunction with dense networks  
110 Gioncu (1995). However, instabilities of type 1, 2 and 3 cannot be observed  
111 by using simple cells, simplified static schemes or the equivalent continuum  
112 method. Therefore, in the general case, the assessment of the load bearing  
113 capacity of a grid-shell relies on performing numerical non-linear buckling  
114 analyses: the so called ‘direct’ method. In particular, the Finite Element  
115 Analysis (FEM) proves to be very effective as it allows to:

- 116 • analyse any shape, also free-form shapes;
- 117 • point out buckling of all types;
- 118 • take into account the effect of imperfections;
- 119 • observe the softening behaviour (geometrical non-linearity);
- 120 • introduce material non-linearity.

121 Therefore we performed systematic geometrically non-linear analyses with  
122 a commercial FEM software Oasys Software (2012). Details are given in  
123 section 5.1. In particular, we chose not to consider material non-linearity  
124 because of the higher computational time needed and the large number of  
125 analyses performed. Indeed it is likely that the failure mode of grid-shells,  
126 especially if free-form, would be affected by yielding of the beams material  
127 (as is the case for the British Museum Great Court roof, for example). But

128 the purpose of this study is not that of assessing the real buckling load  
129 of a grid-shell, but rather only that of estimating the buckling strength of  
130 the Statics Aware Voronoi Grid-Shells in comparison with their state-of-the-  
131 art competitors. For this reason, we have deemed geometrically non-linear  
132 analyses to be accurate enough for our aim.

### 133 3. Imperfection sensitivity analysis

It is well-known that the solution of the generalized eigenvalue problem:

$$det(\mathbf{K}) = det(\mathbf{K}_e + \lambda\mathbf{K}_\sigma) = 0 \quad (1)$$

134 where  $\mathbf{K}$  is the initial global stiffness matrix,  $\mathbf{K}_e$  is the initial global elastic  
135 stiffness matrix,  $\mathbf{K}_\sigma$  is the global geometric stiffness matrix and  $\lambda$  is the load  
136 factor that amplifies the external loads, provides an overestimate of the real  
137 buckling load. This is especially the case for shells and grid-shells endowed  
138 with a high level of symmetry, where imperfection sensitivity and modes  
139 buckling interaction may even halve the theoretical buckling load Hutchinson  
140 (1967). This happens because these kind of structures are characterized  
141 by a high membrane to bending strain energy ratio, and this in turn makes  
142 them very sensitive to imperfections Schmidt (2000). The process of evalu-  
143 ating the effects of imperfections on the buckling strength of a structure is  
144 known as imperfection sensitivity analysis, and it is essential in assessing the  
145 safety of efficient structures.

146 Koiter Koiter (1967) elaborated the ‘initial post-buckling theory’, which as-  
147 sumes that it is possible to evaluate the behaviour of the imperfect structure  
148 by knowing the behaviour of the perfect one. It applies to structures showing  
149 bifurcation of equilibrium and lays its foundations on the asymptotical ap-  
150 proximation of the post-buckling path. Unfortunately, it is limited to almost  
151 linear fundamental paths only as well as imperfections of small amplitude.

152 A more recent trend is the ‘minimum perturbation energy’ concept, which  
153 identifies snap-through phenomena towards secondary equilibrium paths by  
154 perturbing the system Dinkler and Pontow (2006); Ewert et al. (2006).

155 Nevertheless, the most commonly adopted method for determining the effect  
156 of imperfections is that of numerically analysing the imperfect model itself,  
157 which is called under the name of ‘direct approach’. This in turn raises the  
158 question of how to compute the ‘worst imperfection’, i.e. that imperfection  
159 that yields the lower buckling factor. It is worth noticing that the problem

160 of finding the worst imperfection shape within a given amplitude limit is also  
161 coupled in the variables shape and amplitude. This search is still an open  
162 problem and some even think it does not have a unique solution Schneider  
163 et al. (2005). Indeed this approach has the advantage that complex searches  
164 for the non-linear post-critical path are avoided, as the introduction of the  
165 imperfections converts bifurcation points into limit points. On the other  
166 hand, it is definitely computationally expensive as it requires to carry out a  
167 series of fully non-linear analyses on a (possibly infinite) set of models adul-  
168 terated with different imperfections. The computational cost is sometimes  
169 discouraging, especially for everyday design. As a consequence, several vari-  
170 ations to the general procedure have been proposed.

171 Deml and Wunderlich Deml and Wunderlich (1997) propose to describe im-  
172 perfections as additional nodal degrees of freedom and to solve for both the  
173 buckling load and the corresponding ‘worst’ imperfection shape by solving  
174 an extended system of nonlinear equations.

175 After the studies of Ho Ho (1972) it was known that the worst imperfec-  
176 tion shape is to be sought after within the convex linear combinations of the  
177 linear eigenmodes (i.e. the eigenvectors  $\mathbf{u}_i$  associated to the solutions  $\lambda_i$  of  
178 equation (1), with  $\mathbf{u}_i^T \mathbf{u}_j = \delta_{ij}$ ). Subsequently it was also observed that in  
179 certain cases, especially when the softening behaviour is much pronounced  
180 in the pre-buckling phase, the worst imperfection shape must also take into  
181 account the non-linear eigenmodes (i.e. the eigenvectors  $\mathbf{u}_i$  associated to the  
182 solutions  $\lambda_i$  of equation (1), with  $\mathbf{K}$  being evaluated just before the bifurca-  
183 tion point) Greiner and Derler (1995).

184 A modern approach of absorbing this knowledge is that of setting up a non-  
185 linear optimization problem in which the solution is sought within convex  
186 linear combinations of linear and non-linear eigenmodes, subjected to user-  
187 defined imperfection amplitude constraints, by minimizing the buckling load  
188 Lindgaard et al. (2010). As expected, it is found out that lower buckling loads  
189 are obtained by considering also non-linear buckling modes and that the worst  
190 imperfection shape is usually composed of several eigenmodes. Additionally,  
191 it is noticed that the first non-linear eigenmode is a very good approximation  
192 of the worst imperfection shape. Nevertheless, it is also common knowledge  
193 that the first linear eigenmode represents a satisfactory approximation as well  
194 CEN (2007), although for some structures higher linear eigenmodes might  
195 erode the load bearing capacity even more Graciano et al. (2011).

196 Kristanic and Korelc Kristanič and Korelc (2008) propose instead a linear  
197 optimization problem, by carefully choosing linear constraints on both the

198 shape and the amplitude of the imperfections. They also include deformation  
199 shapes (i.e. the displacement fields of the structure due to relevant load  
200 cases) among the base shapes for the generation of the convex linear combi-  
201 nations.

202 However, other studies showed that the worst imperfection form depends on  
203 the specific combination of the structure’s geometry and loading. Addition-  
204 ally dimples and local imperfections in general, that are more relevant to  
205 production and may also represent the occurrence of local instabilities along  
206 the loading path, might also cater for the maximum reduction in load bearing  
207 capacity Song et al. (2004); Schneider and Brede (2005). Therefore, eigen-  
208 modes combinations as well as all long-wave imperfections may overestimate  
209 the buckling load. Additionally, it is worth noting that some authors include  
210 also several post-buckling deformed shapes among the competitors for the  
211 worst imperfection shape Song et al. (2004); Schneider (2006).

212 In the light of these results the concept of ‘quasi-collapse-affine imperfec-  
213 tion’ has emerged, together with the awareness that the worst imperfection  
214 shape cannot be pinpointed Schneider et al. (2005). Schneider finds that the  
215 worst imperfection pattern does not exist for shells because it depends on  
216 the imperfection amplitude. Additionally, it cannot be spotted as it relies  
217 heavily on clustering of instability loads, crossing of secondary equilibrium  
218 paths in the post-buckling range and material non-linearity. Therefore he  
219 introduces the concept of ‘quasi-collapse-affine imperfections’: displacement  
220 fields extracted from the initial stage of the buckling process, obtained by  
221 conveniently restricting the space of the shape functions. These imperfec-  
222 tions turn out to be more unfavourable than eigenmodes, especially when  
223 the instability is caused also by material non-linearity. Actually they initiate  
224 the buckling process (they ‘stimulate’ it) thus allowing to approach the most  
225 unfavourable imperfection pattern Schneider (2006).

226  
227 Most of the described contributions are specific to shells, whereas few  
228 references specific to grid-shells are available. Bulenda and Knippers Bulenda  
229 and Knippers (2001) propose to adopt as imperfection shapes the non-linear  
230 eigenmodes and the displacement shapes of the grid-shell under relevant load  
231 cases.

232 We use GSA as a FE-program Oasys Software (2012), a commercial soft-  
233 ware which does not allow the user to check and manipulate the stiffness  
234 matrix. Thus we can neither obtain non-linear eigenmodes nor restrict the  
235 space of the shape functions in order to compute ‘virtual’ initial buckling



236 shapes (as proposed by Schneider Schneider (2006)). However, our study  
 237 is a parametric analysis on the imperfection sensitivity of grid-shells with  
 238 different topology (i.e., triangular, quadrilateral and hex-dominant), and not  
 239 a thorough assessment of the safety of real projects. All this being said,  
 240 we content ourselves with ‘stimulating’ the buckling process as proposed by  
 241 Schneider Schneider et al. (2005); Schneider (2006), by adopting the following  
 242 imperfections shapes (see Figure 2 for an example):

- 243 1. the displacement shape obtained by linear static analysis, addressed  
 244 with the acronym *LS* in the following;
- 245 2. the initial buckling shape obtained by geometrically non-linear analysis  
 246 (i.e. the ‘real quasi-collapse-affine’ imperfection according to Schneider  
 247 Schneider et al. (2005); Schneider (2006)), addressed with the acronym  
 248 *NLS* in the following;
- 249 3. the first linear eigenmode and convex linear combinations of the first ten  
 250 linear eigenmodes, addressed with the acronym *LB* in the following. No  
 251 optimization procedure is established: the generic *i*-th buckling mode is  
 252 only included when a visual resemblance is noticed with the non-linear  
 253 initial buckling shape of the grid-shell (i.e. *NLS*).

254 It is once again worth noticing that, as this is a comparative analysis and not  
 255 a real project, only the dead load case has been considered. No asymmetric  
 256 load cases have been addressed, neither in the buckling analyses nor in the  
 257 definition of the imperfection shapes.

258 For each dataset (see Table 1), for each topology and for each imperfec-  
 259 tion shape, we have created a range of imperfect models by varying both  
 260 the norm of the imperfection and its sign. The norm is Euclidean ( $\|\mathbf{e}\|_2 =$   
 261  $\sqrt{\sum_i (e_{ix}^2 + e_{iy}^2 + e_{iz}^2)}$ ) and it was sampled at regular intervals  $\pm[250\ 200\ 150\ 100\ 50\ 25\ 0]$   
 262 mm. Every time the imperfections shapes have been scaled according to the  
 263 selected maximum norm and added to the perfect geometry. We have also  
 264 taken into account the sign of the imperfections, as it may significantly in-  
 265 fluence the buckling behaviour of the grid-shell.

266 In so doing, we ended up with a total of 13 imperfect models for each im-  
 267 perfection shape, for each topology and for each dataset, for a total of more  
 268 than 400 models (see second column of Table 1). Each model has then been  
 269 analysed with the GSA FE-program Oasys Software (2012), by carrying out  
 270 geometrically non-linear buckling analyses (see section 2 for reasons about  
 271 neglecting material non-linearity and section 5.1 for details about modeling

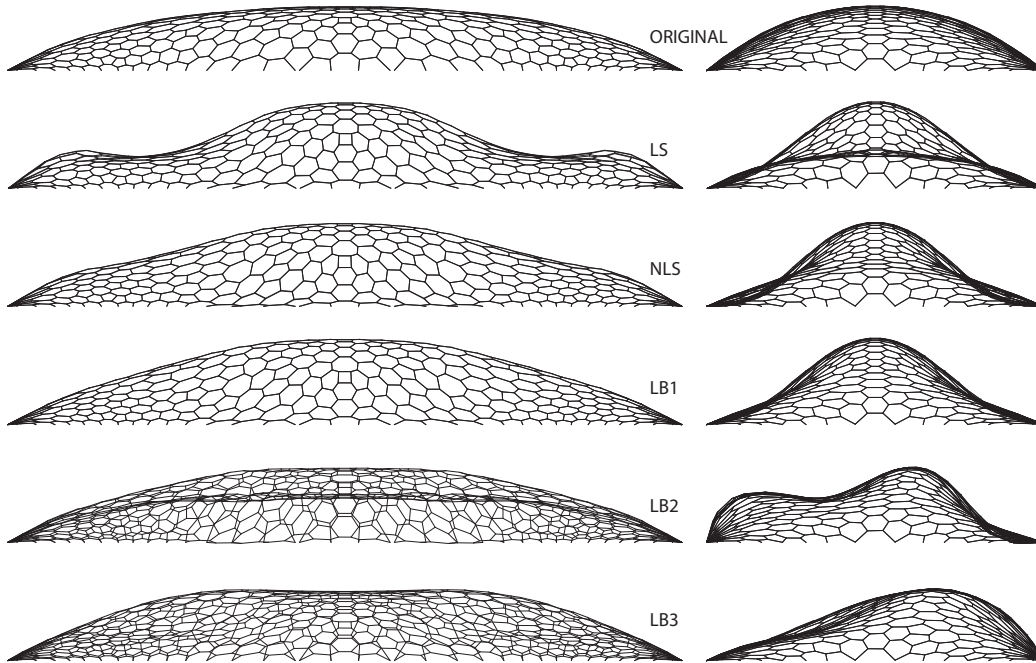


Figure 2: Magnified deformed shapes for the hex-dominant remeshing of the Neumünster dataset, side and front views. From top to bottom respectively: ORIGINAL, LS, NLS, 1st LB eigenmode, 2nd LB eigenmode and 3rd LB eigenmode.

272 and load cases). Imperfection sensitivity diagrams are shown in Figure 6,  
 273 whereas relevant load-deflection diagrams are displayed in Figure 7.

#### 274 4. Statics aware Voronoi remeshing

275 Here we briefly report the method we use to design the Statics Aware  
 276 Voronoi Grid-Shells. Our method is based on *Anisotropic Centroidal Voronoi*  
 277 *Tessellations (ACVT)* Du et al. (1999) and it is driven by the statics of the  
 278 input surface, aiming at improving the strength of the grid-shell as well as  
 279 its aesthetics.

280 Voronoi diagrams appear in nature in many forms. In several cases, such  
 281 as in the porous structure of animal bones, Voronoi-like structures optimize  
 282 strength while keeping a light weight. We follow a similar approach to design  
 283 hex-dominant grid-shells, by concentrating more cells of smaller size in zones  
 284 subject to higher stress, while aligning the elements of our grid to the maxi-  
 285 mum stress direction. The pipeline of the method is summarised in Figure 3

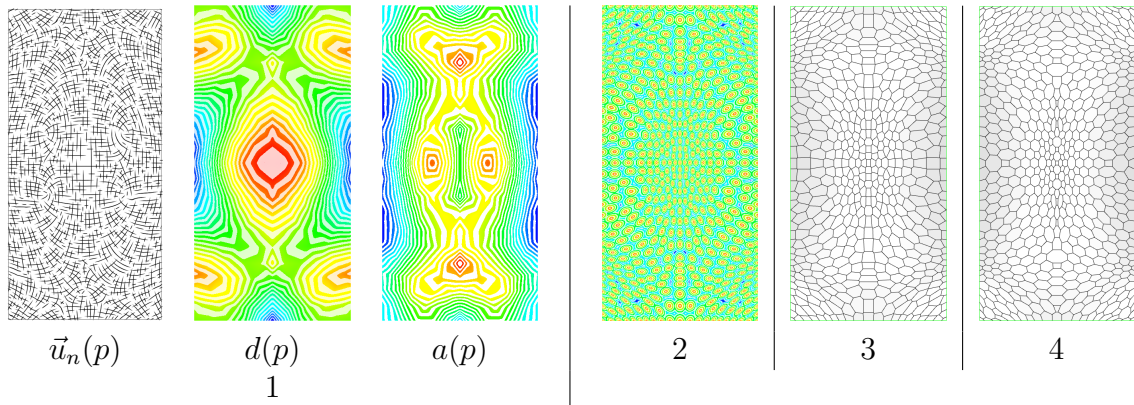


Figure 3: The different steps composing the pipeline of Pietroni et al. (2015): the components of the stress tensor inducing the anisotropic metric (1); the distribution of seeds and their distance field (2); the corresponding ACVT (3); the final optimized tessellation (4).

286 and briefly discussed below. The reader is referred to Pietroni et al. (2015)  
 287 for further details.

288 Given an initial surface  $\Sigma$  we first perform a linear static analysis of the  
 289 continuous shell under dead load (although in theory every load condition  
 290 can be adopted), thus obtaining a stress tensor for each point  $p \in \Sigma$ . As a  
 291 thin shell can be considered in a plane stress condition, the resulting stress  
 292 tensor is two-dimensional. Therefore we express it with respect to the local  
 293 principal directions and we represent it as a pair of mutually orthogonal line  
 294 fields<sup>1</sup>  $\Psi(p) = (\vec{u}(p), \vec{v}(p))$ , where  $\vec{u}$  and  $\vec{v}$  define the maximum and minimum  
 295 principal stresses at each point of the surface, respectively. Since  $\vec{u}$  and  $\vec{v}$   
 296 are orthogonal, we decouple the scalar and directional information and represent  
 297  $\Psi$  as a triple  $(\vec{u}_n(p), d(p), a(p))$ , where  $\vec{u}_n$  is a unit-length vector parallel to  
 298  $\vec{u}$ ,  $d = |\vec{u}|$  is the maximum stress intensity (henceforth called *density*), and  
 299  $a = |\vec{u}|/|\vec{v}|$  is the *anisotropy* (see Figure 3.1). Tensor  $\Psi$  induces an anisotropic  
 300 metric  $g_\Psi = \text{diag}(\frac{1}{d^2}, \frac{a^2}{d^2})$  on surface  $\Sigma$ , where the matrix is expressed with  
 301 respect to the principal reference system at  $p$ .

302 Next we compute a hex-dominant tessellation covering  $\Sigma$ , whose faces  
 303 have a uniform distribution with respect to metric  $g_\Psi$ . Roughly speaking, this

<sup>1</sup>A line field is a vector field modulo its orientation: only the directions and sizes of  $\vec{u}$  and  $\vec{v}$  are relevant to  $\Psi$ , not their orientations.

304 means that faces will be more dense where the maximum stress is higher and  
305 they will be elongated along the direction of maximum stress proportionally  
306 to anisotropy.

307 In order to do so, we sample a set of seeds on the surface Massimiliano  
308 (2012) , and then we relax their positions so that the distribution of seeds  
309 becomes uniform with respect to metric  $g_\Psi$ . Relaxation consists of comput-  
310 ing the Voronoi diagram of the seeds under metric  $g_\Psi$  and iteratively moving  
311 each seed to the centroid of its Voronoi cell Valette and Chassery (2004), un-  
312 til convergence. Note that, since  $g_\Psi$  has variable density and is anisotropic,  
313 the distribution of seeds will not be uniform with respect to the Euclidean  
314 metric: Figure 3.2 depicts the distribution of seeds (red dots) together with  
315 the corresponding field that encodes distance of points on the surface from  
316 the seeds; Figure 3.3 depicts the corresponding ACVT, which assembles the  
317 (anisotropic) Voronoi cells of all seeds and is easily computed from the dis-  
318 tance field.

319 Finally, we apply geometric optimization to improve the local shape of  
320 the faces of the hex-dominant mesh. Roughly speaking, we deform each face  
321 to its closest regular polygon under metric  $g_\Psi$  and we globally optimise the  
322 mesh by stitching adjacent polygons. The result of optimisation is depicted  
323 in Figure 3.4.

## 324 5. Experimental setup

325 We have tested our method on several input surfaces. Figure 1 shows  
326 the rendered views of the hex-dominant remeshing of these surfaces (i.e. the  
327 Statics Aware Voronoi Grid-Shells), whereas Figure 4 compares the top views  
328 of the various remeshings of each input surface. A summary of the datasets  
329 is presented in Table 1:

- 330 1. *Neumünster Abbey* is the glass roof of the courtyard of the Neumünster  
331 Abbey in Luxembourg, designed by RFR-Paris RFR-Paris (2003) and  
332 built in 2003;
- 333 2. *British Museum* is the great court glass roof in the British Museum: ge-  
334 ometry rationalization by Prof. Chris J. K. Williams Williams (2001),  
335 structural design by Buro Happold and construction completed in 2000  
336 by Waagner Biro;
- 337 3. *Aquadom* and *Lilium Tower* are architectural free form shapes; the  
338 latter is the top of the Lilium Tower skyscraper designed by Zaha Hadid

Dataset	Model	Vertices' Valence	Vertices	Faces	Edges	Beams' section (mm)	Total length
<i>Neumünster Abbey</i>	Triangular RFR-Paris (2003)	6	220	380	541	CS $\phi$ 60	966
	Quadrilateral	4	508	464	883	CS $\phi$ 60	932
	Voronoi	3	1076	553	1522	CS $\phi$ 60	956
<i>British Museum</i>	Triangular Williams (2001)	6	1746	3312	4878	CHS 120x30	1026
	Quadrilateral	4	4693	4452	8723	CHS 120x30	1018
	Voronoi	3	10221	5784	14829	CHS 120x30	1031
<i>Aquadom</i>	Quadrilateral Vouga et al. (2012)	4	1078	1001	1936	CHS 100x20	3672
	Voronoi	3	2382	1189	3400	CHS 100x20	3662
<i>Lilium Tower</i>	Quadrilateral Vouga et al. (2012)	4	665	636	1244	CHS 100x20	2139
	Voronoi	3	1432	717	2060	CHS 100x20	2121

Table 1: Statistics on datasets. When a reference is given the remeshing comes from that source, otherwise it is a height field isotropic remeshing  $s(x, y)$ .

339 architects. The quadrilateral remeshings for these datasets come from  
340 the statics optimization procedure of Vouga et al. (2012).

341 *Neumünster* and *British Museum* datasets represent lightweight, quite ordi-  
342 nary surface geometries and very low height-to-span ratio grid-shells, whereas  
343 *Aquadom* and *Lilium Tower* embody architectural free form skins as well as  
344 high height-to-span ratio grid-shells.

### 345 5.1. Restraints, load conditions, numerical modelling

346 Since this is a comparative analysis and not a specific study on the topic  
347 of stability of grid-shells, some simplifications have been done:

- 348 1. All models have *pin joints* all over the boundary. This is a strong as-  
349 sumption as the boundary support can have a tremendous influence  
350 over the structure's behaviour.

351 The theory of bending of surfaces in the large proved that ovaloids (i.e.  
352 closed convex surfaces with positive Gaussian curvature everywhere)  
353 are rigid: i.e. they do not admit any infinitesimal bending except  
354 from motions do Carmo (1976). Cohn-Vossen then proved that every  
355 ovaloid becomes non-rigid if any portion of it is removed Alexandrov  
356 (1947); Calladine (1983); Rayleigh (1890): i.e. it can undergo no more  
357 extensional deformation only but also inextensional deformation (i.e.  
358 bending).

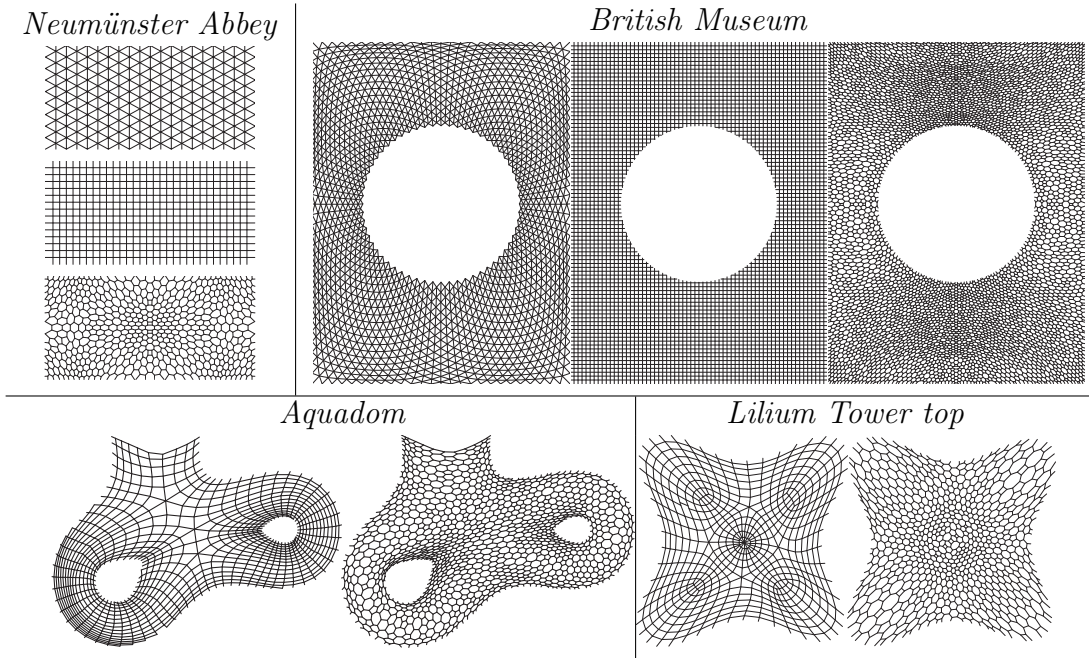


Figure 4: Top views of all remeshings utilised in our comparative analysis.

359  
360  
361  
362  
363  
364  
365  
366  
367  
368  
369  
370  
371  
372  
373  
374  
375  
376

A shell, those with synclastic surface at least, can be regarded as a broken ovaloid whereas its restraints can be considered as devices aimed at restoring the surface continuity. It is evident that the higher the degree of restraint the more rigid the shell will be. Nevertheless, no clear relationship is available in literature relating the stiffness of a shell to its degree of restraint.

Things may become even trickier for grid-shells, where variables like grid topology, grid-spacing and grid-orientation come into play. It is not a case that often the grid generation step takes the cue from both the boundary shape and the restraint condition. Just to cite a relevant example, the geometry of the British Museum triangular grid-shell has been generated with respect to a given specific support condition: i.e. sliding bearings together with tension beams along the edges, resisting the thrust at the corners.

All this being said, we understand that modeling a single type of restraint case does not allow us to study the relationship between grid-shell topology and restraint condition. We also understand that assuming a single unvaried support condition for all the models may put

377 some of them at disadvantage, as their geometry often arises from a  
378 specific set of supports.

379 Nevertheless we reckon that such a simplification is necessary due to  
380 the great amount of variables already involved in our analysis. Further  
381 studies will be required to address this topic;

- 382 2. The beams' joints are modeled as rigid;
- 383 3. The beams' size varies according to the specific model (as is shown in  
384 Table 1) but it is constant within each model;
- 385 4. The beams' cross section is always circular, either solid or hollow (see  
386 Table 1).

387 The shape of the cross section determines the ellipse of inertia of the  
388 beam and hence its bending and torsional stiffnesses. While a trian-  
389 gular mesh resists in-plane shear mostly by means of extensional stiff-  
390 ness, the in-plane equilibrium of polygonal grids relies heavily on both  
391 bending and torsional stiffnesses of the mesh beams and hence in turn  
392 on the beams' cross section. This topic is thoroughly addressed and  
393 developed in Tonelli (2014), where the equivalent membrane stiffness,  
394 bending stiffness and thickness are analytically evaluated for the regu-  
395 lar tilings of the Euclidean plane (i.e. isotropic triangular, quadrilateral  
396 and hexagonal grids).

397 For the sake of this analysis, we have stuck to circular cross sections  
398 only because they are reasonably representative of the compact cross  
399 sections which are currently adopted in the design and construction  
400 of grid-shells Schlaich and Schober (1994, 1996, 1997); Bulenda and  
401 Knippers (2001);

- 402 5. The load is always uniformly distributed (i.e. dead load). Three load  
403 cases have been considered, respectively:
  - 404 (a)  $G_1$  which is the dead load of the beams;
  - 405 (b)  $G_2$  which is a uniform projected load of  $0.75 \text{ kN/m}^2$  of magnitude,  
406 that stands for an hypothetical 25 mm thick glass coverage;
  - 407 (c)  $Q_k$  which is a uniform projected load of  $1.00 \text{ kN/m}^2$  of magnitude,  
408 that represents the snow action.

409 Then a serviceability load combination  $q = 1.0G_1 + 1.0G_2 + 1.0Q_k$  is  
410 used to carry out all the analyses;

- 411 6. Material non-linearity is neglected as the analyses already involve many  
412 variables (see section 2 for further explanations);
- 413 7. Each beam is modeled as a single finite element in order to reduce the  
414 computational time, while keeping an acceptable level of accuracy of

415 the overall simulation. This simplification prevents from pointing out  
416 single member buckling, but it is still acceptable as member buckling  
417 is not the ordinary failure mode for grid-shells.

## 418 5.2. Statics comparison criteria

419 As we want to assess the structural performances of the Statics Aware  
420 Voronoi Grid-Shells, we set up a comparative evaluation with respect to other  
421 current practices (e.g. triangular and quadrilateral remeshing schemes).

422  
423 As a basic criterion, equivalent grid-shells must be characterized by the  
424 same overall structural mass. Therefore in the following the total mass of  
425 the structure is considered constant.

426 Also, in order to minimize the number of variables involved, the shape of the  
427 members cross section must be kept constant for all the topologies.

428 Nevertheless, as roughly stated by Gioncu Gioncu (1995) and Malek  
429 Malek and Williams (2013), the structural performance of a grid-shell with  
430 fixed topology is not only affected by the total weight of its members but also  
431 by its grid-spacing. Giving a coherent definition of grid-spacing for grid-shells  
432 with different geometry and topology is not a straightforward matter though.

433  
434 As a first attempt, for grid-shells with isotropic and equi-area cells only,  
435 one could argue that the grid-spacing could be defined as the bare *edge length*.  
436 It is evident though that different topologies are characterized by different  
437 *area / perimeter* ratios. This in turn means that each topology requires a  
438 different total number of cells as well as an overall different total length of  
439 members to cover a given surface. Together with the aforementioned con-  
440 straints of fixed overall structural mass and beams' shape, this definition of  
441 grid-spacing leads also to grid-shells with different members size.

442 Similarly and more generically, for isotropic but non equi-area grid-shells  
443 (i.e. adaptive grids, whose cells area may vary locally), the *average edge*  
444 *length* might be assumed as a measure of the grid-spacing.

445  
446 In order to check the consequences of such a definition of grid-spacing we  
447 set up a bespoke numerical experiment, whose results are shown in Figure 5.  
448 A grid-spacing sensitivity analysis has been carried out on a shallow spherical  
449 cap (60 m of span and 2.8 m of height) remeshed with isotropic triangular,  
450 quadrilateral and Voronoi-like topology, respectively. Solid circular beams  
451 with tailored radia have been assigned to each remeshing in order to keep



452 the total mass always constant.  
 453 The grid-spacing represented on the  $x$ -axis of the diagram is defined as the  
 454 edge length for the isotropic triangular and quadrilateral topologies and as  
 455 the average edge length for the Voronoi topology.  
 456 By increasing the grid-spacing the overall members length decreases, while  
 457 the total mass is kept constant (see above).  
 458 Looking at the graph of Figure 5 it is seen that the load factor varies with  
 459 the grid-spacing. More importantly, the very gap in terms of load bearing  
 460 capacity of grid-shells of different topology varies with the grid-spacing. This  
 461 in turn means that the choice of an arbitrary grid-spacing (e.g. edge length)  
 462 for our parametric studies on the buckling strength of grid-shells with differ-  
 463 ent topologies would randomly affect the outcome of the experiments.

464  
 465 In light of these results we enforce the constancy of both total mass  
 466 and total remeshing length as a sound criterion for generating ‘statically  
 467 equivalent’ grid-shells with different topologies.  
 468 Therefore, concluding, two grid-shells with different topology share the same  
 469 *overall grid-spacing* when they are characterized by the some total remeshing  
 470 length.

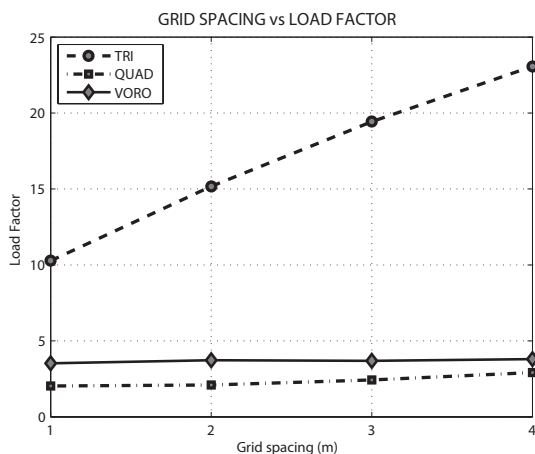


Figure 5: Results of grid-spacing sensitivity analyses on a spherical cap surface (span-to-height ratio = 21.43). For this surface the triangular connectivity is the most sensitive to grid-spacing variations, as its load bearing capacity rockets as grid-spacing increases.

471 **6. Results**

472 We have compared the triangular, quadrilateral and Statics Aware Voronoi-  
473 like patterns in terms of buckling strength, stiffness and imperfection sensi-  
474 tivity. In particular, the following comparisons have been performed:

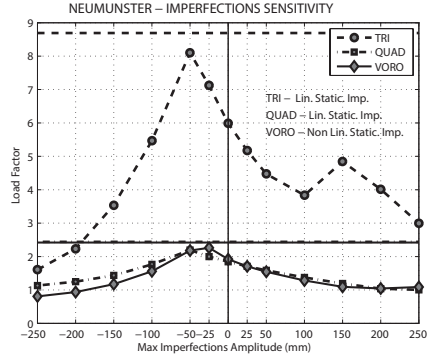
475 **Imperfection sensitivity analysis:** this analysis shows how the buckling  
476 factor is affected by surface, grid-topology and imperfections shape,  
477 sign and amplitude (see Figure 6 for results and section 3 for the setup  
478 of imperfect models).

479 **‘Worst’ response diagram vs Grid-topology:** for each dataset (i.e. for  
480 each surface analysed, see first column of Table 1) this study compares  
481 the ‘worst’ response diagram (i.e. that corresponding to the lowest  
482 load factor) of each grid-topology (see Figure 7 for results - the state  
483 parameter on  $x$  axis represents the vertical deflection of the black bullet  
484 depicted in Figure 1).

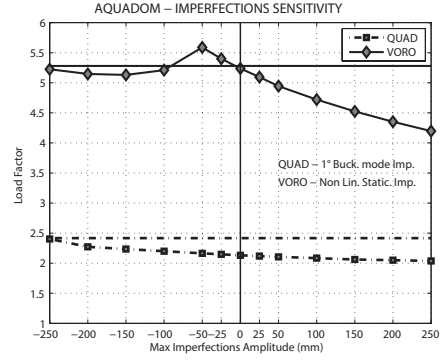
485 **Response diagram vs Imperfection amplitude:** this study outlines the  
486 variability of the response diagram with the signed magnitude of the  
487 (worst) imperfection shape (see Figure 8 for results). For the sake of  
488 brevity, only the results concerning the triangular and Statics Aware  
489 Voronoi remeshings of the *Neumünster* dataset are reported.

490 *6.1. Comparative imperfection sensitivity analysis*

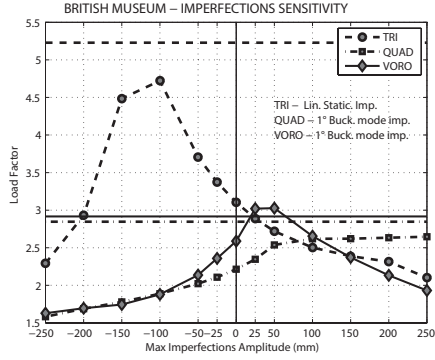
491 Some theoretical background may help framing the results obtained into  
492 a more generic context. To this aim, Figure 6(e) and 6(f) describe two kinds  
493 of critical points: an unstable symmetric bifurcation point and a limit point  
494 Thompson and Hunt (1984), respectively. A structure characterized by an  
495 unstable symmetric bifurcation point displays a decreasing critical load for  
496 whatever imperfection is applied to its geometry, no matter the type nor the  
497 magnitude. In jargon the curve describing the variation of the structures’  
498 critical load with the imperfection shape and magnitude is called two-thirds  
499 power law cusp (see Thompson and Hunt (1984) and Figure 6(e)-right). On  
500 the other hand, a structure characterized by a limit point shows either an  
501 increase or a decrease of its buckling load according to the sign of the imper-  
502 fection applied to it. This behaviour is well summarized by the monothonic  
503 non-singular curve represented in Figure 6(f)-right.



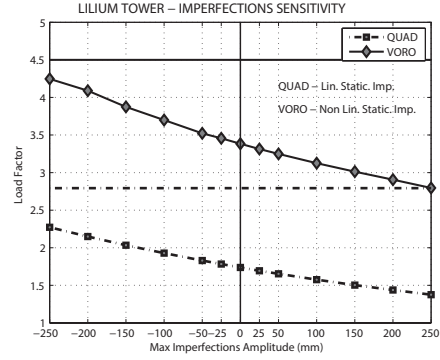
(a) Neumünster



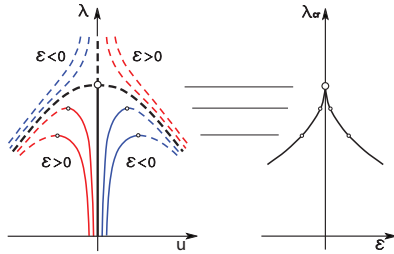
(b) Aquadom



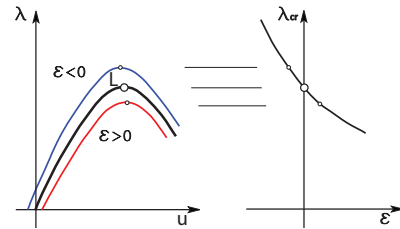
(c) British Museum



(d) Liliun Tower



(e) Unstable symmetric bifurcation point



(f) Limit point

Figure 6: Imperfection sensitivity results. On the left column, from top to bottom: *Neumünster Abbey* courtyard glass roof, *British Museum* great court roof and schematic representation of an unstable symmetric bifurcation point. On the right column, from top to bottom: *Aquadom*, *Lilium Tower* and schematic representation of a limit point. The horizontal lines in Figures (a)-(d) represent the first linear eigenvalue (i.e. buckling load) computed on the corresponding perfect model. Text within the graphs of Figures (a)-(d) recalls the ‘worst’ geometric imperfection shape which generates the graphs (see section 3 for terminology).

504 A quick inspection of these curves provides a satisfactory insight in the sta-  
505 bility of the structure at hand. In fact, the stability behaviour of most part of  
506 lightweight compressive structures such as grid-shells can be usually related  
507 to one of those curves.

508 Therefore we have graphed the outcome of our geometrically non-linear anal-  
509 yses in  $\lambda - \varepsilon$  charts (i.e. critical load *vs* imperfection), in order to relate the  
510 various structural behaviours encountered to one of the aforementioned cat-  
511 egories.

512 In accordance with Section 1, Figure 6 shows that the triangular topology  
513 is definitely the most effective as well as the most sensitive to imperfections  
514 (see Figures 6(a) and 6(c)), followed by our Statics Aware Voronoi remesh-  
515 ing (Figures 6(c) and 6(b)), while the quadrilateral pattern turns out to be  
516 the less sensitive to imperfections. These numerical results are in full accor-  
517 dance with the theoretical predictions of Tonelli Tonelli (2014), which where  
518 partially sketched in Sections 1 and 5.1.

519 Additionally, it is also evident that the regularity of the surface plays a  
520 central role in the definition of the critical point. According to section 5,  
521 Neumünster and British Museum datasets represent rather regular geome-  
522 tries (the former more regular than the latter, see Figures 1 and 4) whereas  
523 Aquadom and Liliun Tower Top are free-form surfaces. Figures 6(a) and 6(c)  
524 show that the Neumünster and British Museum datasets display an *unstable*  
525 *symmetric bifurcation point* Thompson and Hunt (1984) (compare the graphs  
526 with the two-thirds power law cusp of Figure 6(e)) roughly irrespective of  
527 the topology, although the trend is much more noticeable for the triangular  
528 topology. Similarly, Figures 6(b) and 6(d) show that free-form surfaces such  
529 as Aquadom and Liliun datasets display a *limit point* Thompson and Hunt  
530 (1984) (compare the graphs with the monotonic non-singular curve of Figure  
531 6(f)), again irrespective of the topology.

532 Another clear result provided by Figure 6 is that the Statics Aware  
533 Voronoi topology is just as efficient as the quadrilateral topology when the un-  
534 derlying surface is quite regular (Neumünster and British Museum datasets,  
535 respectively Figures 6(a) and 6(c)) but its efficiency is even more than twice  
536 that of the quadrilateral pattern when the underlying surface becomes irreg-  
537 ular or totally free-form (Aquadom and Liliun datasets, respectively Figures  
538 6(b) and 6(d)).

539 Contrary to polar-symmetric domes (which exhibit a symmetric graph  
540 both for negative and positive imperfections Bulenda and Knippers (2001)),  
541 none of the tested grid-shells show a symmetric behaviour with respect to

542 the imperfection sign. Hence, the *sign of imperfections* plays a crucial role  
 543 in the structural behaviour of grid-shells. Besides, the singularity of the cusp  
 544 representative of the unstable symmetric bifurcation point of Figures 6(a)  
 545 and 6(c) does never correspond to the perfect model. This in turn means  
 546 that the perfect grid-shell does not necessarily produce the highest buckling  
 547 factor (it never does in our experiments). Therefore, in certain circumstances,  
 548 a slight imperfection acts as a mild stiffening for the grid-shell.

549 As a last remark, at least under dead load, the ‘worst’ imperfection shape  
 550 is topology-dependent. It is seen that, among the imperfection shapes taken  
 551 into account (see section 3 for details and terminology), the ‘worst’ is:

- 552 1. the first linear eigenmode  $LB$  for triangular topology (see Figures 6(a),(c));
- 553 2. either the first linear eigenmode  $LB$  or the linear static displacement  
 554 shape  $LS$  for the quadrilateral topology (see Figures 6(b),(c) and 6(a),(d),  
 555 respectively);
- 556 3. the initial buckling shape of the perfect model  $NLS$  for the statics aware  
 557 Voronoi-like topology (see Figures 6(a),(b),(d)).

558 According to section 3, other convex combinations of linear eigenmodes have  
 559 been considered, but in no case any of these has come out as the ‘worst’  
 560 imperfection shape. Unfortunately, in agreement with Bulenda and Knippers  
 561 Bulenda and Knippers (2001), from our sensitivity analysis no relationship  
 562 between imperfection shape and amplitude can be worked out in order to  
 563 predict the ‘worst’ imperfection.

## 564 6.2. Comparative analysis of ‘worst’ response diagram vs Grid-topology

565 Figure 7 shows the ‘worst’ response diagrams for each grid-topology (i.e.  
 566 triangular, quadrilateral and Statics Aware Voronoi-like) of each dataset (first  
 567 column of Table 1). As usual, the term ‘worst’ response diagram means that  
 568 it is associated with the imperfect model which produces the lowest load  
 569 factor.

570 As expected, triangular grid-shells achieve the highest load factor together  
 571 with the lowest deformation (see Figures 7(a) and 7(b)). As already outlined  
 572 in sections 1 and 6.1, the triangular topology is together the strongest as well  
 573 as the most stiff, to such an extent that it does not require any stiffening  
 574 device.

575 On the contrary, almost all of the polygonal grid-shells (i.e. quadrilateral  
 576 and Statics Aware Voronoi-like) exhibit a very much pronounced softening  
 577 behaviour prior to collapse. They fail when a local maximum is reached along

578 the primary equilibrium path, but by then they have undergone extremely  
579 high (totally unsatisfactory) forerunner displacements. Roughly speaking,  
580 they behave like thick equivalent continuous shells made of a ‘squashy’ ma-  
581 terial (i.e. with low equivalent Young modulus), according to the analytical  
582 results of Tonelli Tonelli (2014). It is worth noticing that this happens irre-  
583 spective of the regularity of the underlying surface, i.e. there is no distinction  
584 between regular datasets such as Neumünster and British Museum and free-  
585 form datasets such as Aquadom and Liliium (just compare the scale of the  
586 horizontal axis in Figures 7(a),(b) and 7(d)). These huge displacements point  
587 out the need for the adoption of an appropriate stiffening method, aimed at  
588 reducing the flexibility.

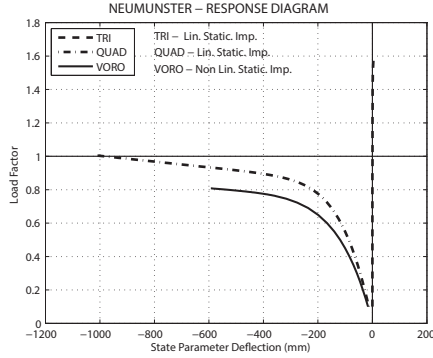
589 Indeed, polygonal lattice shells exhibit a proper shell behaviour only when a  
590 suitable stabilizing system is introduced. Usually a bracing cable system is  
591 used that caters for the shear forces to be transferred by membrane action,  
592 whereas transverse diaphragms might be added in order to provide for the  
593 double curvature to be maintained Schlaich and Schober (2002).

594 Eventually, as already pointed out in section 6.1, the Statics Aware  
595 Voronoi remeshing becomes very effective for architectural free-form surfaces  
596 with a high height-to-span ratio (i.e. *Aquadom* and *Liliium Tower* datasets).  
597 Indeed, it achieves buckling factors which are on average twice as much as  
598 those yielded by equivalent quadrilateral state-of-the-art grid-shells (see Fig-  
599 ures 7(c) and 7(d)). This excellent result is due both to the innate adaptivity  
600 of the Voronoi diagram and to the ‘*statics awareness*’ introduced by Pietroni  
601 et al. Pietroni et al. (2015).

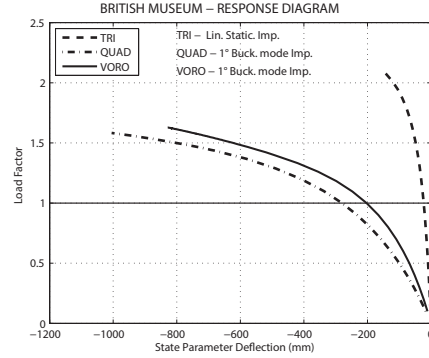
### 602 6.3. Response diagram vs Imperfection amplitude

603 Figure 8 illustrates the variation of the response diagram with the signed  
604 amplitude of the imperfection for the Neumünster dataset. For the sake of  
605 brevity, only the triangular and Statics Aware Voronoi-like topologies are  
606 reported with reference to their ‘worst’ imperfection shape (i.e. the *LS* and  
607 *NLS* imperfections, respectively - see Figure 6(a)).

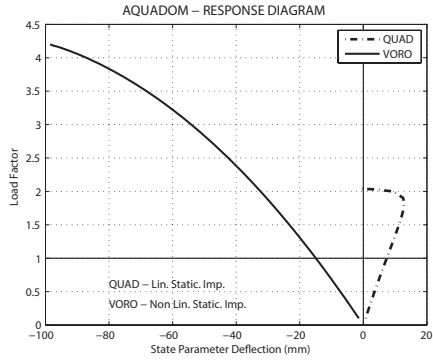
608 It is evident that there is no straightforward correlation between the im-  
609 perfection amplitude and the shape of the response diagram. It is also worth  
610 mentioning that GSA Oasys Software (2012) works in load control, which  
611 in turn means that it is not able to follow the post-buckling behaviour (e.g.  
612 also the potential bifurcation point of the triangular pattern). A correlation  
613 is instead spotted between the trend of the diagrams of Figure 8 and those  
614 of Figure 6(a). In particular, the cusp points of Figure 6(a) correspond to a



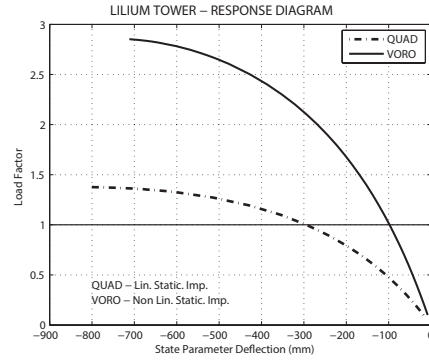
(a) Neumünster



(b) British Museum



(c) Aquadom



(d) Lilium Tower

Figure 7: ‘Worst’ response diagrams *vs* Grid-topology. Respectively from top left to bottom right: *Neumünster Abbey* courtyard glass roof, *British Museum* great court roof, *Aquadom* and *Lilium Tower* datasets. The horizontal solid lines represent the ‘safety’ unit load factor. Text within the graphs recalls the ‘worst’ geometric imperfection shape which generates the diagrams (see section 3 for terminology). The state parameter referred to on the  $x$  axis is the vertical deflection of the black bullet depicted in Figure 1.

615 sensible snap-back and an almost infinite slope in the corresponding response  
 616 diagrams of Figures 8(a) and 8(b), respectively. In so doing, the cusp points  
 617 of Figure 6(a) can be regarded as ‘boundary lines’ (red lines in Figure 8) in  
 618 the response diagram *vs* imperfection amplitude graphs of Figure 8.

619 Eventually, the triangular topology displays a rather linear behaviour up  
 620 to collapse (or up to the 80% of the collapse load at least) on average. On the  
 621 contrary, the Statics Aware Voronoi-like topology exhibits a sensible softening  
 622 ing behaviour along the loading process, that intensifies as the imperfection

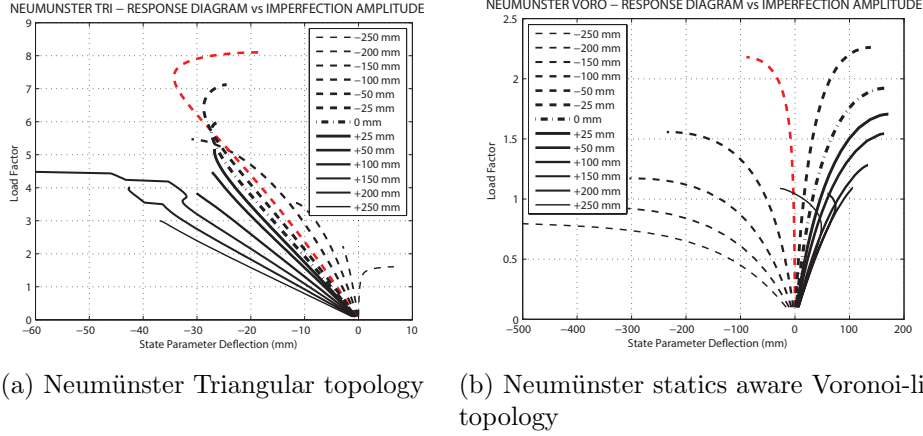


Figure 8: Variation of the response diagram with the signed amplitude of the imperfection for the *Neumünster* dataset. On the left the triangular remeshing, on the right our statics aware Voronoi remeshing. The state parameter referred to on the  $x$  axis is the vertical deflection of the black bullet depicted in Figure 1.

623 amplitude grows.

624 Unfortunately, there are no evident rules on how to state in advance  
 625 the load-deflection relation for a whatsoever imperfect structure. Then the  
 626 engineer has to undergo all the efforts of a thorough imperfection sensitivity  
 627 analysis, as the response diagram shape affects the safety of the structure.

## 628 7. Statics-Aware Voronoi Mock-up

629 A mock-up of Statics Aware Voronoi Grid-Shell has been built at the  
 630 Department D.E.S.T.e.C. of the University of Pisa, with overall dimensions  
 631 (2.4x2.4x0.7)m and composed of 465 joints, 697 beams and 231 panels (see  
 632 Figure 9 and Table 2 for statistics).

633 The joints were 3D printed, the timber beams manually cut and the P.E.T.  
 634 panels laser cut. All the geometry was digitally handled by means of Rhinoceros  
 635 Becker and Golay (1999), in particular using its plug-in RhinoScript for au-  
 636 tomating some procedures. During the assembling phase (lasted 17 days)  
 637 temporary ‘scaffoldings’ were needed until the structure was completed and  
 638 could bear its own weight (see Figure 9).



	<i>Beams</i>	<i>Joints</i>	<i>Faces</i>	<i>Washers</i>	<i>Screws</i>
Number	697	231	465	227	243
Material	Mild Fir	ABS	PET	Iron	Iron
$\rho$ ( $\frac{kg}{m^3}$ )	400	1050	1400	7750	7750
$M_{tot}$ (kg)	1.5	1.6	7.2	2.5	0.3
$M_{tot}$ (kg)	13.1				

Table 2: Statistics on the mock-up.

## 639 8. Conclusions

640 This paper tackles the problems of the assessment of the structural per-  
641 formance of a novel hex-dominant remeshing pattern for free-form grid-shells:  
642 the *Statics Aware Voronoi Remeshing* scheme introduced by Pietroni et al.  
643 Pietroni et al. (2015).

644 The basic intuition for the generation of the geometry is to lay out the beams  
645 network along the edges of an Anisotropic Centroidal Voronoi tessellation of  
646 the surface, where the metric used is not the Euclidean metric but that in-  
647 duced by the stress tensor over the surface under dead load.

648  
649 In order to assess their structural capabilities we have carried out a sys-  
650 tematic comparative analysis between them and equivalent state-of-the-art  
651 competitors (i.e. grid-shells with triangular and quadrilateral topology). To  
652 this aim, we have performed extensive investigations through numerical ge-  
653 ometrically non-linear analyses. The results we have obtained show that,  
654 at least with respect to the specific conditions addressed (i.e. dead loading,  
655 rigid joints, pinned boundary etc...), our free-form Statics Aware Voronoi  
656 Grid-Shells are not only aesthetically pleasing but also statically efficient.  
657 Obviously they cannot be as efficient as the triangular grid-shells, but they  
658 turn out to be twice as effective as their equivalent state-of-the-art quadri-  
659 lateral competitors. Therefore they may indeed represent a valid alternative  
660 for the design of modern grid-shells, especially if the underlying surface is  
661 free-form. In particular we have observed that the bigger the irregularity of  
662 the underlying surface, the better the structural performances of our Statics  
663 Aware Voronoi Grid-Shells thanks to the *statics awareness* supplied by the  
664 statically driven metric.

665 This indeed holds true when the Statics Aware Voronoi Grid-shells are sub-  
666 ject to uniform load cases (e.g. gravity load). On the other hand further  
667 research should be carried out in order to assess their effectiveness under

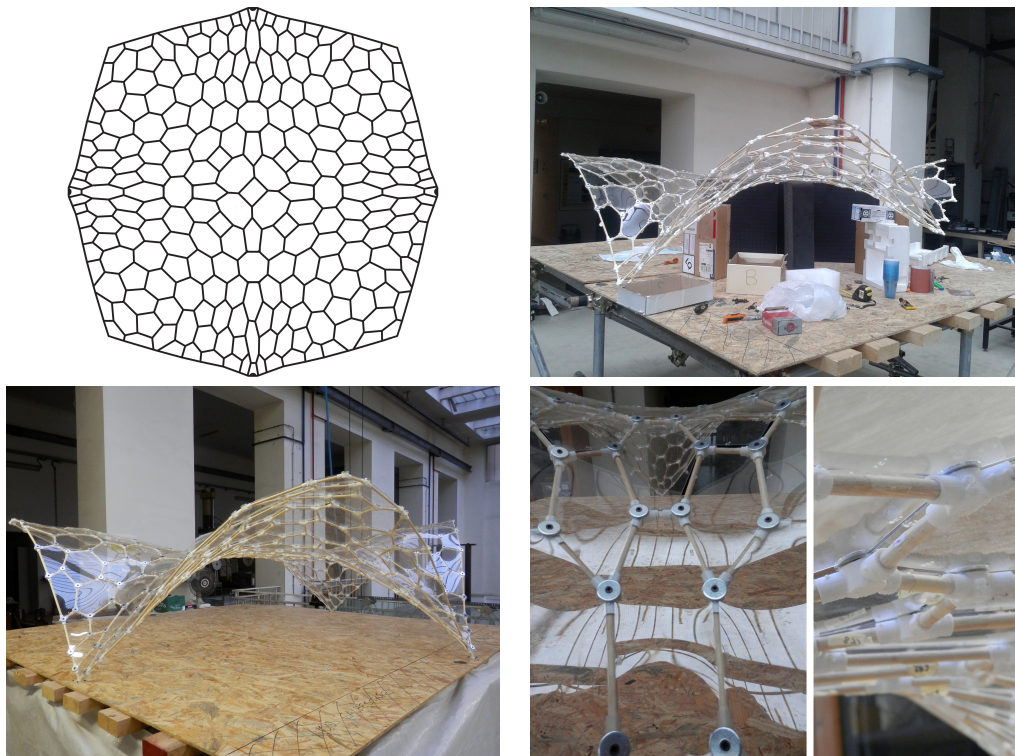


Figure 9: The geometry of the Statics Aware Voronoi Grid-Shell mock-up.

668 different load conditions. In particular anti-metric load cases are envisaged  
 669 to be extremely detrimental because, as it stands, the Statics Aware Voronoi  
 670 remeshing algorithm generates optimal grid-shells with respect to symmetric  
 671 loading only.

672 These situations are exactly those in which a prospective stiffening device  
 673 should kick in, bringing about much needed stiffness. The analysis of such  
 674 a complex and detailed device is out of the scope of the present study and  
 675 need to be addressed separately.

676 Also, to this respect, the stiffness of the joints plays a very important role on  
 677 the overall behaviour of the grid-shell. Generally speaking a grid-shell with  
 678 all pinned nodes is a mechanism whereas the same grid-shell with rigid joints  
 679 usually yields the best performances. Nevertheless seldom rigid joints can  
 680 be achieved in practice and therefore a systematic study would be required  
 681 in order to assess the effect of the stiffness of the joints over the grid-shell  
 682 behaviour. Again, the analysis of such a delicate matter requires extensive

683 research and as such is clearly out of the scope of the present work.

684

685 A thorough imperfection sensitivity analysis has also been carried out. We  
686 have found out that the ‘worst’ imperfection shape is topology-dependent, i.e.  
687 it varies with the remeshing pattern even if the underlying surface is kept  
688 constant. In particular, the initial buckling shape proposed by Schneider  
689 Schneider et al. (2005); Schneider (2006) under the name of ‘quasi-collapse-  
690 affine’ imperfection seems to be the most unfavourable imperfection for the  
691 Statics Aware Voronoi grid-shells. Additionally, although less sensitive to  
692 imperfections than shells, the reduction of the buckling load might be very  
693 high also for grid-shells. Specifically, the stiffer they are the higher their  
694 collapse load abatement is.

695 In particular, the failure load of imperfect triangular grid-shells can be even  
696 a quarter of the theoretical value, Statics Aware Voronoi grid-shells can have  
697 their buckling load halved whereas quadrilateral grid-shells are usually the  
698 least sensitive with a maximum fall of 35% (see Figure 6). Again, these  
699 results hold true for grid-shells subject to uniform loading only and hence  
700 further research should be carried out to extend them to different load con-  
701 ditions (e.g. anti-metric loading).

702

703 From a geometrical and pragmatic standpoint, Statics Aware Voronoi  
704 meshes have twice the number of vertices with respect to statically equivalent  
705 quadrilateral meshes (see section 5.2), but at the same time all vertices have  
706 valence three (see Table 1), thus they are competitive from the feasibility  
707 viewpoint too.

708 At this stage of development the Statics Aware Voronoi Remeshing algorithm  
709 does not yield planar faces, thus it is not directly applicable to the design  
710 of glass-covered grid-shells. Nevertheless with further focused research we  
711 are confident that a face single curvature constraint could be implemented.  
712 This in turn would pave the way for the use of rigid cladding materials such  
713 as cold-bent glass Belis et al. (2007); Eekhout and Staaks (2007); Vakar and  
714 Gaal (2004), GRP, GRC etc... For further details about planarity of the faces  
715 and geometric aspects, the reader is referred to Pietroni et al. (2015).

716 Adriaenssens, S., Block, P., Veenendaal, D., Williams, C. (Eds.), April 2014.  
717 Shell Structures for Architecture: Form Finding and Optimization. Taylor  
718 and Francis - Routledge, London.

- 719 Alexandrov, A. D., 1947. On the works of S. E. Cohn-Vossen. *Upsehi Matem.*  
720 *Nauk* 2 (3(19)), 107–141.
- 721 Becker, M., Golay, P., 1999. *Rhino NURBS 3D Modeling*. No. v. 1. New  
722 Riders.
- 723 Belis, J., Inghelbrecht, B., Van Impe, R., Callewaert, D., 2007. Experimental  
724 assessment of cold-bent glass panels. *Glass Performance Days, Tamglass*  
725 1, 115–117.
- 726 Bulenda, T., Knippers, J., 2001. Stability of grid shells. *Computers and*  
727 *Structures* 79 (12), 1161 – 1174.
- 728 Calladine, C. R., 1983. *Theory of shell structures*. Cambridge University  
729 Press, Cambridge, Cambridgeshire, New York, includes index.  
730 URL <http://opac.inria.fr/record=b1091215>
- 731 CEN, 2007. Eurocode 3: Design of Steel Structures. Part.  
732 1-6: Strength and Stability of Shell Structures. CEN,  
733 <https://law.resource.org/pub/eur/ibr/en.1993.1.6.2007.html>.
- 734 Deml, M., Wunderlich, W., 1997. Direct evaluation of the ‘worst’ imperfec-  
735 tion shape in shell buckling. *Computer Methods in Applied Mechanics*  
736 *and Engineering* 149 (1–4), 201 – 222, containing papers presented at the  
737 Symposium on Advances in Computational Mechanics.  
738 URL <http://www.sciencedirect.com/science/article/pii/S0045782597000558>
- 739 Dinkler, D., Pontow, J., 2006. A model to evaluate dynamic stability of  
740 imperfection sensitive shells. *Computational Mechanics* 37 (6), 523–529.  
741 URL <http://dx.doi.org/10.1007/s00466-005-0729-7>
- 742 do Carmo, M. P., 1976. *Differential geometry of curves and surfaces*. Prentice  
743 Hall.
- 744 Du, Q., Faber, V., Gunzburger, M., Jan. 1999. Centroidal Voronoi Tessella-  
745 tions: Applications and Algorithms. *SIAM Review* 41 (4), 637–676.  
746 URL <http://epubs.siam.org/doi/abs/10.1137/S0036144599352836>
- 747 Eekhout, M., Staaks, D., 2007. Cold Deformation of Glass. *Glass Perfor-*  
748 *mance Days* -, –.

- 749 Ewert, E., Schweizerhof, K., Vielsack, P., 2006. Measures to judge the sen-  
750 sitivity of thin-walled shells concerning stability under different loading  
751 conditions. *Computational Mechanics* 37 (6), 507–522.  
752 URL <http://dx.doi.org/10.1007/s00466-005-0733-y>
- 753 Forman, S. E., Hutchinson, J. W., 1970. Buckling of reticulated shell struc-  
754 tures. *International Journal of Solids and Structures* 6 (7), 909 – 932.
- 755 Gioncu, V., 1995. Buckling of Reticulated Shells: State-of-the-Art. *Internation-  
756 al Journal of Space Structures* 10, 1–46.
- 757 Glymph, J., Shelden, D., Ceccato, C., Musse, J., Schober, H., 2004. A para-  
758 metric strategy for free-form glass structures using quadrilateral planar  
759 facets. *Automation in Construction* 13, 187–202.
- 760 Graciano, C., Casanova, E., Martínez, J., 2011. Imperfection sensitivity of  
761 plate girder webs subjected to patch loading. *Journal of Constructional  
762 Steel Research* 67 (7), 1128 – 1133.  
763 URL <http://www.sciencedirect.com/science/article/pii/S0143974X11000459>
- 764 Greiner, R., Derler, P., 1995. Effect of imperfections on wind-loaded  
765 cylindrical shells. *Thin-Walled Structures* 23 (1–4), 271 – 281, buckling  
766 Strength of Imperfection-sensitive Shells.  
767 URL <http://www.sciencedirect.com/science/article/pii/0263823195000167>
- 768 Ho, D., 1972. The influence of imperfections on systems with coincident buck-  
769 ling loads. *International Journal of Non-Linear Mechanics* 7 (3), 311 – 321.  
770 URL <http://www.sciencedirect.com/science/article/pii/0020746272900534>
- 771 Hutchinson, J. W., 1967. Imperfection sensitivity of externally pressurized  
772 spherical shells. *Journal of Applied Mechanics* 34, 49–55.
- 773 Jiang, C., Wang, J., Wallner, J., Pottmann, H., 2014. Freeform honeycomb  
774 structures. *Computer Graphics Forum* 33 (5), Proc. Symp. Geom. Process-  
775 ing.
- 776 Koiter, W., 1967. On the stability of elastic equilibrium. NASA technical  
777 translation. National Aeronautics and Space Administration.
- 778 Kristanič, N., Korelc, J., 2008. Optimization method for the determination of  
779 the most unfavorable imperfection of structures. *Computational Mechanics*

- 780 42 (6), 859–872.  
781 URL <http://dx.doi.org/10.1007/s00466-008-0288-9>
- 782 Lindgaard, E., Lund, E., Rasmussen, K., 2010. Nonlinear buckling opti-  
783 mization of composite structures considering “worst” shape imperfections.  
784 *International Journal of Solids and Structures* 47 (22–23), 3186 – 3202.  
785 URL <http://www.sciencedirect.com/science/article/pii/S0020768310002738>
- 786 Liu, Y., Pottmann, H., Wallner, J., Yang, Y.-L., Wang, W., 2006. Geometric  
787 Modeling with Conical Meshes and Developable Surfaces. *ACM Transac-*  
788 *tions on Graphics* 25, 681–689.
- 789 Malek, S., Williams, C. J. K., 23-27 September 2013. Structural implications  
790 of using cairo tiling and hexagons in gridshells. Wroclaw, Poland, pro-  
791 ceedings of the International Association for Shell and Spatial Structures  
792 (IASS) Symposium 2013 - “Beyond the Limits of Man”.
- 793 Massimiliano, C., 2012. Efficient and flexible sampling with blue noise prop-  
794 erties of triangular meshes. *IEEE Transactions on Visualization and Com-*  
795 *puter Graphics* 18 (6), 914–924.
- 796 Oasys Software, 2012. GSA Version 8.6 reference manual. Arup, 13 Fitzroy  
797 Street London.
- 798 Pietroni, N., Tonelli, D., Puppo, E., Froli, M., Scopigno, R., Cignoni, P.,  
799 2015. Statics aware grid shells. *Computer Graphics Forum* 34 (2), 627–  
800 641.  
801 URL <http://dx.doi.org/10.1111/cgf.12590>
- 802 Rayleigh, L., 1890. On Bells. *The London, Edinburgh and Dublin Philosoph-*  
803 *ical Magazine and Journal of Science* (5).
- 804 RFR-Paris, 2003. Neumünster abbey glazing, neumünster luxembourg.
- 805 Schlaich, J., Schober, H., 1994. Glass-covered lightweight spatial structures.  
806 pp. 1–27.
- 807 Schlaich, J., Schober, H., 1996. Glass-covered grid-shells. *Structural Engi-*  
808 *neering International: Journal of the International Association for Bridge*  
809 *and Structural Engineering (IABSE)* 6 (2), 88–90.

- 810 Schlaich, J., Schober, H., 1997. Glass roof for the hippo house at the berlin  
811 zoo. *Structural Engineering International: Journal of the International*  
812 *Association for Bridge and Structural Engineering (IABSE)* 7 (4), 252–  
813 254.
- 814 Schlaich, J., Schober, H., 2002. Design principles of glass roofs. pp. 815–827,  
815 proceedings of the International Symposium on Lightweight structures in  
816 civil engineering, Warsaw, Poland.
- 817 Schmidt, H., 2000. Stability of steel shell structures: General report. *Journal*  
818 *of Constructional Steel Research* 55 (1–3), 159 – 181.  
819 URL <http://www.sciencedirect.com/science/article/pii/S0143974X9900084X>
- 820 Schneider, W., 2006. Stimulating equivalent geometric imperfections for the  
821 numerical buckling strength verification of axially compressed cylindrical  
822 steel shells. *Computational Mechanics* 37 (6), 530–536.  
823 URL <http://dx.doi.org/10.1007/s00466-005-0728-8>
- 824 Schneider, W., Brede, A., 2005. Consistent equivalent geometric imperfec-  
825 tions for the numerical buckling strength verification of cylindrical shells  
826 under uniform external pressure. *Thin-Walled Structures* 43 (2), 175 – 188.  
827 URL <http://www.sciencedirect.com/science/article/pii/S0263823104001648>
- 828 Schneider, W., Timmel, I., Höhn, K., 2005. The conception of quasi-collapse-  
829 affine imperfections: A new approach to unfavourable imperfections of  
830 thin-walled shell structures. *Thin-Walled Structures* 43 (8), 1202 – 1224.  
831 URL <http://www.sciencedirect.com/science/article/pii/S0263823105000583>
- 832 Song, C., Teng, J., Rotter, J., 2004. Imperfection sensitivity of thin elastic  
833 cylindrical shells subject to partial axial compression. *International*  
834 *Journal of Solids and Structures* 41 (24–25), 7155 – 7180.  
835 URL <http://www.sciencedirect.com/science/article/pii/S0020768304002756>
- 836 Sumec, J., Zingali, A., 1987. A study of the influence of initial shape imper-  
837 fections on the stability of lattice shells by direct and shell analogy method.  
838 *International journal of space structures* 2, 223–230.
- 839 Thompson, J., Hunt, G., 1984. *Elastic Instability Phenomena*, 1st Edition.  
840 John Wiley & Sons, Inc., New York, NY, USA.

- 841 Timoshenko, S. P., Gere, J. M., 1961. Theory of elastic stability. McGraw-Hill  
842 classic textbook reissue. McGraw-Hill, 1988, New York, reprint. Originally  
843 published: 2nd ed. New York : McGraw-Hill, 1961. (Engineering societies  
844 monographs).
- 845 Tonelli, D., 2014. Statics Aware Voronoi Grid-Shells. Ph.D. thesis, University  
846 of Pisa.  
847 URL <https://etd.adm.unipi.it/theses/available/etd-03052015-154257/>
- 848 Vakar, L., Gaal, M., 2004. Cold Bendable, Laminated Glass - New Possibili-  
849 ties in Design. Structural Engineering International (SEI) 14 (2), 95–97.
- 850 Valette, S., Chassery, J.-M., Sep. 2004. Approximated Centroidal Voronoi  
851 Diagrams for Uniform Polygonal Mesh Coarsening. Computer Graphics  
852 Forum 23 (3), 381–389.  
853 URL <http://doi.wiley.com/10.1111/j.1467-8659.2004.00769.x>
- 854 Vouga, E., Höbinger, M., Wallner, J., Pottmann, H., 2012. Design of self-  
855 supporting surfaces. ACM Trans. GraphicsProc. SIGGRAPH.
- 856 Weingarten, V. I., Seide, P., Peterson, J. P., 1968. Buckling of thin-walled  
857 circular cylinders. Tech. rep., NASA.
- 858 Williams, C. J. K., 3-5 August 2001. The analytic and numerical definition  
859 of the geometry of the british museum great court roof. Deakin Unversity,  
860 Geelong, Australia, pp. 434–440, proceedings of the Third International  
861 Conference on Mathematics & Design, M&D.
- 862 Wright, D. T., 1965. Membrane forces and buckling in reticulated shells.  
863 Journal of the Structural Division 91 (1), 173–202.